Eur. Phys. J. Plus (2025) 140:166
https://doi.org/10.1140/epjp/s13360-025-06095-5

THE EUROPEAN PHYSICAL JOURNAL PLUS

Regular Article

Study of compositional and luminescence properties of calcite in lapis lazuli for provenance investigations of archaeological findings

Marta Magalini[1,2], Laura Guidorzi[1,2], Alessandro Re[1,2,a], Miriana Marabotto[2,3], Alessandro Borghi[4], Paolo Gallo[5], Massimo Vidale[6], Leonardo La Torre[7], Matteo Campostrini[7], Quentin Lemasson[8,9], Laurent Pichon[8,9], Brice Moignard[8,9], Claire Pacheco[8,9], Pierre Couture[10], Vladimir Palitsin[10], Alessandro Lo Giudice[1,2]

[1] Dipartimento di Fisica, Università di Torino, Via Pietro Giuria 1, Turin, Italy
[2] INFN Sezione di Torino, Via Pietro Giuria 1, Turin, Italy
[3] Dipartimento di Elettronica e Telecomunicazioni, Politecnico di Torino, Corso Duca degli Abruzzi 24, Turin, Italy
[4] Dipartimento di Scienze Della Terra, University of Turin, Via Valperga Caluso 35, Turin, Italy
[5] Dipartimento di Studi Storici, University of Turin, Via S. Ottavio 20, Turin, Italy
[6] Dipartimento dei Beni Culturali: Archeologia, Storia dell'Arte, del Cinema e della Musica, Università degli Studi di Padova, Piazza Capitaniato 7, Padua, Italy
[7] INFN Laboratori Nazionali di Legnaro, Viale dell'Università 2, Legnaro, Italy
[8] Centre de Recherche et de Restauration des Musées de France, C2RMF, 14 Quai François Mitterrand, Paris, France
[9] UAR 3506 Lab-BC (CNRS, Ministère de La Culture, Chimie ParisTech), 14 Quai François Mitterrand, Paris, France
[10] Ion Beam Centre, Advanced Technology Institute, University of Surrey, Guildford, Surrey GU2 7XH, UK

Received: 22 November 2024 / Accepted: 4 February 2025

Abstract In this study, calcite crystals within 42 lapis lazuli reference rocks coming from four distinct mining regions (in present-day Afghanistan, Tajikistan, Siberia and Myanmar) were characterised in terms of their compositional and luminescence properties in order to identify potential provenance markers. A non-destructive approach based on Ion Beam Analysis was employed, in particular using μ-Particle Induced X-rays Emission (μ-PIXE) and μ-Ion Beam Induced Luminescence (μ-IBIL). The results indicate that calcite crystals in Afghan rocks are characterised by the highest quantity of Mg and Mn; whereas, Siberian calcite exhibit the highest Sr content. The application of Principal Component Analysis also enhanced the possibility of discriminating between the Myanmar and Tajik rocks, as well as between the four provenances in general, by exploiting the compositional variability of Mg, Mn, Sr and Y elements. Regarding the luminescence properties, notable differences in the intensity ratio between the 360 nm and the 620 nm luminescence bands were detected among the provenances. In the second part of this study, the new results were employed to infer the origin of the raw material of certain archaeological findings discovered in two different historical sites: four lapis lazuli fragments from Shahr-i Sokhta (Iran, 3rd millennium BCE) and a lapis lazuli tessera from the city of Tanis (Egypt, 1050–700 BCE). The results of the analysis indicate that, among the four provenances considered in the reference rocks database, the best compatibility of the data from both case studies is found with the Afghan dataset. This suggests that the area of Afghanistan is the most probable source for the raw materials of the investigated findings.

1 Introduction

Ion Beam Analysis (IBA), and in particular μ-Particle Induced X-rays Emission (μ-PIXE) and μ-Ion Beam Induced Luminescence (μ-IBIL) techniques using proton microbeams, have proven to be a highly effective tool for investigating the provenance of lapis lazuli raw material used in artworks and archaeological objects, due to their high sensitivity, non-destructiveness and the possibility to be applied on a micro-scale [1–3]. Lapis lazuli is in fact a highly heterogeneous material; therefore, it is very challenging to identify characteristic features useful for provenance discrimination from the analysis of the entire rock. For this reason, in previous studies, we focussed on the characterisation of single mineral phases in lapis lazuli, in particular diopside, pyrite and wollastonite. This led to the development of a provenance protocol able to distinguish between five different source areas (in present-day Chile, Tajikistan, Afghanistan, Siberia and Myanmar) [3, 4]. The protocol aims at assisting archaeologists in addressing the issue of lapis lazuli sourcing in antiquity by providing a scientific method to differentiate rocks of different origins on the basis of their compositional and luminescence features. Indeed, Afghanistan is widely regarded as the primary source of this semi-precious blue stone in antiquity, although other geological extraction sites have been debated by scholars [5–7]. However, the protocol demonstrated a limited capacity to differentiate between the Myanmar–Afghanistan and Myanmar–Tajikistan groups of reference

[a] e-mail: alessandro.re@unito.it (corresponding author)

Published online: 26 February 2025

rocks. This is due to the fact that, for the aforementioned discriminations, only weaker markers have been identified thus far in the studied mineral phases. Weaker markers are features valid only for one origin, but not necessarily present in all the samples of that origin. Furthermore, although these phases are commonly observed in lapis lazuli rocks, they are not always present concurrently and there could be cases, especially when analysing archaeological samples that have undergone a long period of burial, where they may be present in an altered state. This latter phenomenon is particularly frequent in the case of pyrite crystals [1, 8]. If these conditions occur, the determination of the provenance of the raw material is significantly constrained.

To address these limitations, in this study we expanded the characterisation of the lapis lazuli material to the calcite mineral phase, employing μ-PIXE and μ-IBIL with the aim of identifying new provenance markers. Calcite ($CaCO_3$) is an important accessory mineral of lapis lazuli and it is widespread in the rocks of almost all the different sources, even with different abundances [9]. Moreover, its crystals exhibit a distinctive orange-red luminescence colour that enables a rather fast identification with the cold-cathodoluminescence maps usually acquired on the sample before IBA. In the first part of this study, the outcomes of μ-PIXE and μ-IBIL investigations of calcite crystals present in 42 reference rocks from our database and sourced from 4 distinct mining areas (Tajikistan, Afghanistan, Siberia and Myanmar—Chile was excluded from the investigation due to the existence of an already well-established identification method [2]) are presented. The supplementary discriminating information extracted through the application on Principal Component Analysis (PCA) to the compositional data is also discussed. In the second part of this work, the same methodology is applied to two different archaeological case studies: a set of four lapis lazuli working fragments from Shahr-i Sokhta (Iran, 3rd millennium BCE) and a lapis lazuli tessera from the city of Tanis (Egypt, 1050–700 BCE, capital of the XXI-XXII dynasties). In the case of the tessera, the standard protocol procedure based on diopside and pyrite crystal analysis was also applied in order to cross-validate the outcomes of the calcite analysis. These two case studies will show that the study of calcite is a self-consistent and effective method to gain new information about the most probable provenance, among the ones considered in the database, of the lapis lazuli rock used to carve the investigated archaeological findings. This provenance information will assist archaeologists in gaining a deeper understanding of the mining regions used as suppliers of the material and, indirectly, of the complex trade connections of the two sites with these suppliers.

2 Samples

2.1 Reference rock samples

The study of the calcite mineral phase in lapis lazuli was conducted by analysing 42 reference rocks, sourced from four different mining areas. In total, 14 samples have an Afghan origin (Badakhshan province), 4 come from Tajikistan (Liadjura-Dara, Pamir Mountains), 13 from Siberia (Irkutsk Oblast) and 11 from Myanmar (Mogok, Mandalay region). Information regarding the provenance of the analysed samples collected in our reference rock set can be found in our previous studies [3, 4, 8, 10, 11]. For each sample, from 1 to 4 calcite crystals were analysed, according to the abundances in the sample, for a total of 86 crystals composing the final dataset. Although IBA techniques are also applicable in air on objects of any shape, rock samples were prepared in the form of petrographic sections (ca. 100 μm thickness) to facilitate the analytical process. The flat geometry and the possibility of placing the sections in-vacuum after carbon coating allows the samples to be easily pre-characterised using scanning electron microscopy coupled with microanalysis (SEM–EDX) and cold-cathodoluminescence (cold-CL) microscopy (as discussed in Sect. 3), as well as to carry out measurements in IBA facilities using in-vacuum microbeam lines. The 42 samples were analysed primarily at the AN2000 accelerator of the INFN-LNL laboratories (Legnaro, Italy), but 3 samples were also analysed at the New AGLAE facility (C2RMF, Paris, France), as described in Sect. 3.

2.2 Archaeological samples

The case studies presented as applications of the provenance investigation based on calcite markers belong to two different archaeological contexts. The first case study concerns four samples from Shahr-i Sokhta, an ancient city of the 3rd millennium BCE, located in southeastern Iran. This city was a consumer of high-quality lapis lazuli beads, and, in part, a hub for the trade routes of this semi-precious blue stone towards other towns on the Iranian Plateau and the western markets [7, 12]. The samples are lapis lazuli waste fragments discovered in a lapis lazuli workshop within the city. Due to their lower artistic value, it was possible to apply a more invasive analysis; hence, the fragments have been embedded in epoxy resin and cut to expose the internal part (Fig. 1a). An in-depth study discussing the application of the provenance protocol described in [4] on a larger set of samples from this site and the archaeological implications of its results is under publication [13]. Here, we present only the new provenance information provided by the characterisation of the calcite phase in a subset of those samples that contained calcite crystals suitable for IBA. For each sample, one or two crystals were measured, resulting in a total of six calcite crystals analysed.

The second case study deals with the analysis of a small lapis lazuli tessera (Fig. 1b), from the archaeological site of Tanis (Egypt), which was the capital of the XXI-XXII Egyptian dynasties (1050–700 BCE). The tessera, casually retrieved in the sixties of the XX century in proximity of the royal tombs near the temple of Amun (collection E. Bresciani), was probably a decorative inlay element on a polymateric sanctuary object. This study presents the first provenance investigation of the raw material of this

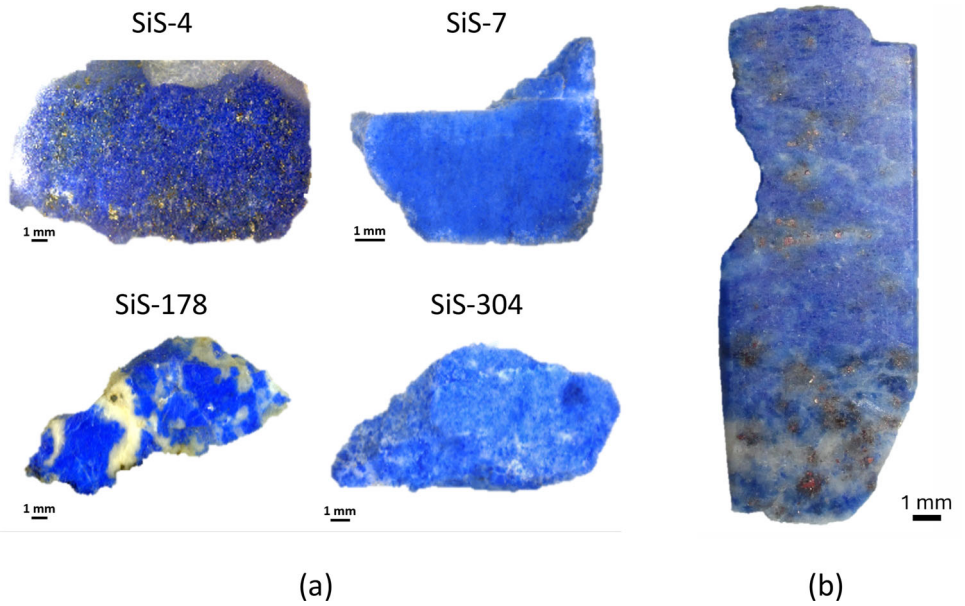

Fig. 1 **a** Lapis lazuli working fragments embedded in resin and polished from Shahr-i Sokhta (3rd millennium BCE, Iran). **b** Lapis lazuli tessera from Tanis (1050–700 BCE, XXI-XXII dynasties), Egypt

tessera and the results will also include the analysis of pyrite and diopside, following the methodology of the provenance protocol. In the tessera from Tanis, two calcite, six pyrite and six diopside crystals were analysed in total.

The analysis on the archaeological samples were conducted at the microbeam lines available at the Surrey Ion Beam Centre (Guildford, UK), at the New AGLAE (Paris, France) or at the INFN-LNL facility, more details about each facility is given in Sect. 3.

3 Instruments and analytical methods

Before applying IBA, reference rocks and archaeological samples were pre-characterised in order to identify the most suitable calcite crystals in terms of composition and dimensions. Regarding the composition of calcite [14], although various divalent cations may partially replace Ca in calcite, many calcite specimens are relatively free from other ions and are fairly close in composition to pure $CaCO_3$. Substitutions which commonly occur include that of Mg. The stability field for magnesian calcites can reach amounts of 20 mol% $MgCO_3$ at high temperature. Manganese-bearing calcites are known with up to 42 mol% $MnCO_3$, and experimental work indicates that calcite with up to 50 mol % $MnCO_3$ can exist. The substitution of Fe^{2+} for some Ca is also fairly common, though iron-bearing calcites are less common than iron-bearing dolomites and members of the ankerite series. Small amounts of Sr commonly substitute for Ca, though Sr is less abundant in calcites than in aragonites, the larger Sr^{2+} ion being more acceptable in the aragonite structure. The composition of the major elements and the absence or scarcity of elements unrelated to calcite were carefully examined, guiding the selection of the crystals in each sample. Furthermore, only the larger-sized crystals were considered to ensure that the proton beam fully remains in the crystal volume, taking into account the diameter, maximum penetration depth ($\sim$37 μm and $\sim$72 μm ranges for 2 and 3 MeV protons, respectively) and lateral straggling of the beam ($\sim$1.5 μm and $\sim$2.6 μm for 2 and 3 MeV, respectively). The calculations of these last two parameters were made using the SRIM software (version 2008.04) [15].

For the pre-characterisation, cold-CL microscopic imaging was employed to map the distribution of the mineral phases present in the sections: calcite crystals are easily detectable by their characteristic orange-red luminescence, in contrast with the yellowish white in diopside and dark blue in lazurite [10]. The instrument employed, hosted at the Earth Science Department of the University of Torino, was a CITL Cold Cathode Luminescence 8200 mk3 instrument equipped with a polarised optical microscope Olympus BH2 and a Peltier-cooled Olympus DP74 camera. The accelerating voltage and current employed during the measurements were 15 kV and 500 μA, respectively. Each CL image was acquired at magnification 2.5 $\times$ and exposition time 50 ms. However, since the dolomite mineral phase ($CaMg(CO_3)_2$) also exhibits a similar red luminescence (although this phase is less common in lapis lazuli rock [9]), SEM–EDX microscopy was also performed on the crystals to verify their correct identification on the basis of their major elements. Two instrumentations were employed in this case: a Zeiss EVO 60 Scanning Electron Microscope equipped with a LaB6 filament and a Bruker Quantax 200 EDX microprobe, working at variable pressure (50 Pa) and with a voltage set at 20 kV, hosted at the scientific laboratories of the Centro Conservazione e Restauro “La Venaria Reale”, Venaria Reale (Italy) and a Scanning Electron Microscope (JEOL JSM-IT300LV) equipped with an Oxford Instruments SDD energy-dispersive X-ray spectrometer (EDX), working in-vacuum and with a voltage set at 15 kV, hosted at the Earth Science Department of the University

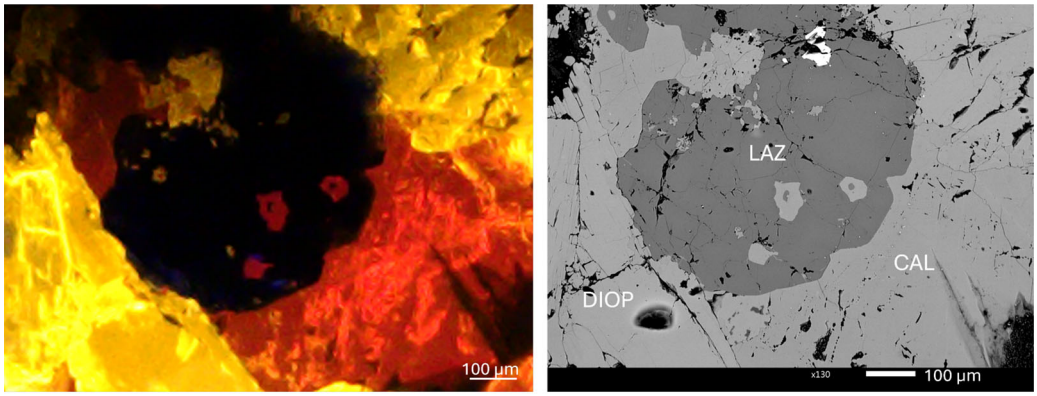

Fig. 2 **a** Example of the map obtained by cold-CL microscopy on a section of lapis lazuli. Calcite/dolomite crystals are easily identified by their red luminescence. **b** Example of the SEM-BSE image of the same area, with identification of mineral phases (*DIOP* diopside, *LAZ* lazurite, *CAL* calcite)

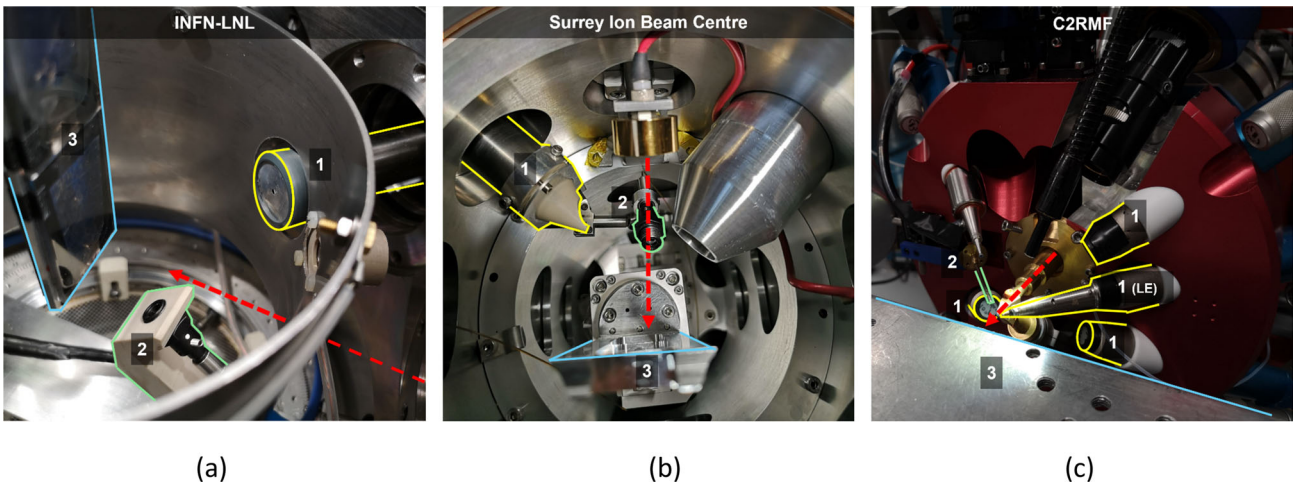

Fig. 3 Microbeam analysis chambers of the LNL-AN2000 accelerator **a**, the Surrey Ion Beam Centre **b**, and the external microbeam line of the New AGLAE accelerator **c**. 1 = PIXE detectors, outlined in yellow; 2 = IBIL setup, outlined in green; 3 = sample holder, outlined in light blue. The red arrow represents the direction of the incoming proton beam. All the details about the instrumentations are listed in Table 1

of Turin. Figure 2 shows an example of a cold-CL map in an area containing a bright red luminescence crystal and the corresponding SEM-BSE image with the mineral phase identification obtained by the microanalysis.

In the study of the Shahr-i Sokhta fragments, due to some limitations of the energy range during the μ-PIXE analysis at the Ion Beam Centre (Guildford, UK), the JEOL JSM-IT300LV SEM–EDX microscope was also employed for the quantification of the Mg concentration. For each targeted calcite crystal, five to eight points were acquired, and the final estimate of the Mg content was obtained by averaging the various measurements and using standard deviation as the associated error.

μ-PIXE and μ-IBIL measurements were carried out at three different research facilities: the INFN-LNL AN2000 in-vacuum microbeam facility (Legnaro, Italy) [16], the Surrey Ion Beam Centre in-vacuum microbeam line (Guildford, UK) [17–20] and the extracted microbeam line at the New AGLAE accelerator (C2RMF, Paris, France) [21, 22]. Table 1 provides a summary of the principal features of the three setups whose photographs are shown in Fig. 3.

With regard to the acquisition modality, at INFN-LNL and Surrey IBC the pre-selected crystals were initially identified by acquiring large and fast PIXE elemental maps. Secondly, maps on uniform areas of $30 \times 30\ \mu m^2$ and $25 \times 25\ \mu m^2$ (depending on the crystal size) were acquired within the crystals for about one hour to gain sufficient statistics to evaluate the trace contents. At New AGLAE, the higher number of detectors allows for a more rapid acquisition of larger areas (e.g. a $500 \times 500\ \mu m^2$ area is scanned in about 10 min); here, large elemental maps are acquired and a post-acquisition selection of sub-areas can be performed using the custom-made software AGLAEMap [23]. In order to reduce the pile-up in the calcite spectra and maximise the signal of interest in the high-energy region, where the provenance marker elements are present, proper absorbers were employed on the detector for the μ-PIXE measurements. However, for the measurements at the Surrey IBC, this limited the detection of light elements, particularly Mg, which was therefore measured with SEM–EDX, as previously explained. The Mg values were employed to recalculate the other elemental concentrations measured with μ-PIXE using a conversion factor to normalise the concentrations to 100 wt% total.

Table 1 General features and experimental conditions for μ-PIXE and μ-IBIL measurements at the different IBA facilities where analysis on lapis lazuli samples were performed.*Nominal beam energy, the energy loss due to the exit window and air thickness is < 1%, negligible for PIXE calculation. **Best performing filter in terms of detectability of trace elements emitting high-energy X-rays (e.g. Sr, Y). *SDD* Silicon Drift Detector, *HPGe* High Purity Germanium Radiation Detectors

		INFN-LNL (Italy)	Surrey ion beam centre (UK)	New AGLAE (France)
General features	Measurement	In vacuum	In vacuum	In air (He flux)
	Ion	Protons	Protons	Protons
	Beam energy (MeV)	2	2	3*
	Average beam current (pA)	800	1000	500
	Beam size (μm)	6–7	5	30–40
μ-PIXE	Detector	1 HPGe (ORTEC IGLET-X)	1 SDD (RAYSPEC SiriusSD)	4 SDD (1 Low Energy (LE) and 3 High Energy (HE)) (KETEK AXAS-M)
	Absorbers	Aluminium funny filter (a)** 113 μm thick, 0.6% hole; (b) 80 μm thick, 8% hole)	130 μm-thick beryllium foil plus 100 μm-thick Kapton film	100 μm -thick Mylar foil for HE
	Acquisition software	OMDAQ 2007	OMDAQ-3 (Oxford Microbeams, Ltd. UK)	AGLAE-ACQ
μ-IBIL	Collimating lens	74-UV (200–2000 nm)	74-UV (200–2000 nm)	-
	Optical fibre(s)	QP600-1-UV–VIS + P600-025-UV–VIS, Ø = 600 μm	MV63L05 Ø = 600 μm	Ø = 1 mm
	Spectrometer	Ocean Optics USB4000	Ocean Optics QEPro	Ocean Optics QE65000
	Bandwidth (nm)	350–1000	250–1200	200–1000
	Resolution (nm)	2	2	3

In order to ensure the compatibility of data acquired with different setups, a set of reference mineral standards (SPI #02753-AB Mineral Standards) was employed for calibration. Furthermore, some lapis lazuli samples prepared as a cross section (about 400 μm thickness) were analysed in all the facilities, confirming the compatibility of the quantitative results obtained with μ-PIXE within two sigma error. The μ-PIXE data acquired at INFN-LNL and Surrey IBC were quantitatively analysed using the GUPIXWIN software (version 2.2.3) [24]; whereas, data from New AGLAE were processed with the custom-made software TRAUPIXE [23], that uses the same GUPIXWIN as calculation engine. All the IBIL spectra were corrected in intensity for the respective instrumental efficiency at different wavelengths. Nevertheless, it was not feasible to conduct a calibration to obtain the absolute luminescence intensity emission, primarily due to the difficulties in realising a calibrated light emitter suitable for all the setups during different measurement runs. Lastly, it should be noted that, due to technical issues, the IBIL spectra were not acquired for all the samples.

4 Results and discussion

4.1 Analysis of reference rocks: μ-PIXE

87 crystals of calcite suitable for IBA were identified with cold-CL and SEM–EDX techniques inside the 42 lapis lazuli reference rocks. μ-PIXE and μ-IBIL were then applied to search for possible provenance markers in different elemental concentration or the presence of characteristic luminescence bands in correlation with the 4 provenances. All the μ-PIXE data are reported in this open access repository on *Zenodo* [25]**.** μ-PIXE analysis showed that the most interesting elements for discrimination are magnesium, manganese, strontium, and yttrium. Figure 4 shows the concentration values of these elements in the form of box plots, grouped according to the different provenances. Mg was found in samples of all the provenances, generally more abundant in Afghan rocks (below 922 (LOD) up to 31,000 ppm) with respect to Siberian (below 785 (LOD) up to 16,200 ppm), Tajik (below 831 (LOD) up to 8600) and Myanmar (from 2200 up to 14,000 ppm) rocks. Similarly, Afghan samples present the major abundance of Mn (from 130 up to 1690 ppm), followed by Siberian (below 28 (LOD) up to 600 ppm), and Tajik (from 140 up to 320 ppm) rocks. In Myanmar rocks the Mn content is generally very low (maximum value 190 ± 40 ppm), and in 11 crystals out of 24 it is below the detection limit (LOD about 30 ppm). Sr was found always above the limit of detection in all the samples, with low values for Tajik (from 240

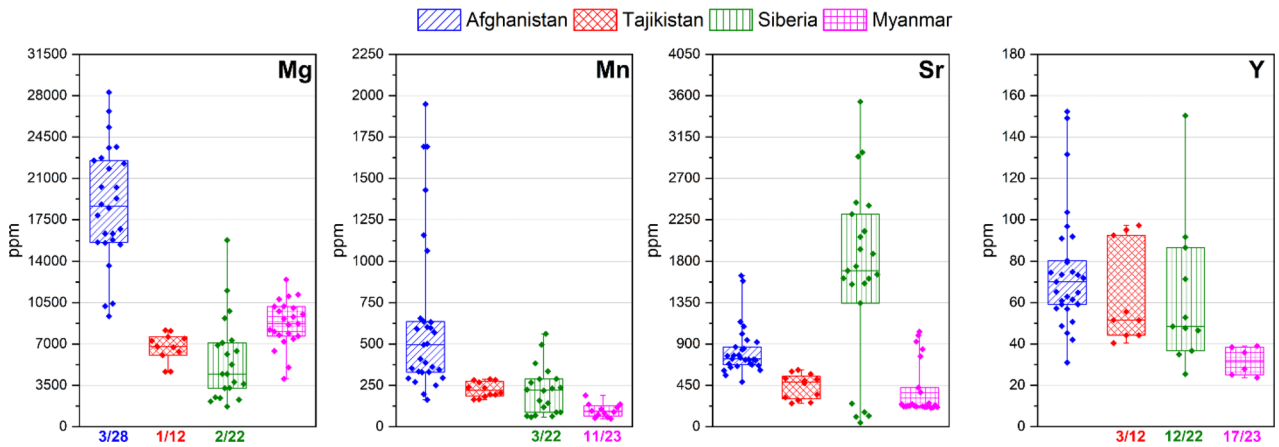

Fig. 4 μ-PIXE results for minor and trace elements concentration in calcite in reference geological samples grouped by provenance area. The box charts represent the dispersion of the experimental points: each point is an individual μ-PIXE measurement on a crystal; the boxes include 50% of analysed points (from 25 to 75%) and are separated in two parts by the median line. In this representation, error bars are not reported to make the graphics more readable; the number of measurements below the limit of detection (LOD) with respect to the total number of crystals measured for each provenance is reported below the x-axis

up to 670 ppm) and Myanmar (from 190 up to 1060 ppm) calcites, intermediate values in Afghan calcites (from 470 up to 1670 ppm) and great abundance in Siberian rocks (from 40 up to 3610 ppm), even if 5 Siberian crystals show values below 300 ppm. It is interesting to notice that these 5 points belong to three different samples that also contain calcite crystals with high abundance of Sr (>1300 ppm). It was observed that Siberian calcite crystals typically exhibit zonation, with the presence of small inclusions having limited Sr content; whereas, the Sr content is typically elevated in the majority of the crystal. This high variability of Sr within the same sample was not observed for the other provenances. Y was found in low quantities in rocks from all the provenances but with different occurrence: more abundant in Afghan rocks (from 25 to 170 ppm), quite abundant in Tajik samples (below 34 (LOD) up to 110 ppm)), whereas under the limit of detection in more than half of the crystals in samples from Siberia (14 over 22, LOD about 30 ppm) and Myanmar (17 over 23, LOD about 16 ppm). In all the previously mentioned ranges, the extremes reported are calculated as one standard deviation below the minimum and above the maximum values. In instances where measurements are present below limit of detection (LOD), the minimum LOD is reported. According to the definition of weaker marker given in the provenance protocol [3], Mg>18,000 ppm and Mn>670 ppm are candidate weaker markers for Afghanistan; whereas, Sr>1740 ppm is a possible weaker marker for Siberia. These thresholds were calculated by summing 3 standard deviations to the respective maximum values of concentration for the Siberian dataset in the case of Mg and Mn, and for the Afghan dataset in the case of Sr. Myanmar and Tajikistan provenances exhibit large overlapping ranges for all elements, although with some differences in the median values. However, it is not feasible to identify net thresholds for differentiating between them. In addition to the elements discussed above, traces of Si, Al, S and, in rare cases, Cu, Zn, As and Rb were also detected, but their distributions do not show significant differences for discriminating between origins. This consideration is also true for Fe, whose presence in calcite is fairly common, and in the analysed dataset it was found always in low concentrations (maximum value 262 ± 7 ppm, in an Afghan sample) and in 49 out of 87 crystals it was under the limit of detection (about 24 ppm).

As demonstrated in a previous study on diopside and pyrite mineral phases in lapis lazuli, a statistical method such as PCA could be a powerful tool to enhance the provenance differentiation by exploiting the correlation between variables (in this case represented by the trace elements) [26]**.** The same custom-made Python script (developed in Spyder 3.3.1 scientific environment [27]) was here adopted to perform PCA on the calcite dataset, using as variables Mg, Mn, Sr and Y. Figure 5a shows the Principal Component 2 (PC2) vs PC1 biplot obtained considering all the 4 provenances. PCA is an unsupervised method, colours are applied for visualisation purpose only at the end of the plotting procedure, and this does not influence the evaluation of the score values. Similarly, the polygons surrounding scores from the same origin serve as visual aids and do not constitute a classification. The overall explained variance covered is 72,6%. PC1, the direction representing the maximum variance in the dataset, receives the biggest contribution from Mn, Y (Mn and Y are positively correlated with each other) and Mg. The Afghan dataset is majorly discriminated from Myanmar and Tajikistan samples along the PC1 direction. Mg also influences the PC2, the component that accounts for the second highest variance in the dataset, together with Sr, but these elements contribute in opposite directions. Y has low weight in the definition to PC2; whereas, Mn is practically irrelevant for this component. The Siberian calcites are majorly separated from the other provenances along this second component except for a small group of points that correspond to the same cluster with low Sr content previously discussed in this section. The Myanmar dataset shows overlaps both with Siberian and Tajik points, but an isolated and dense cluster of points is present at negative values of PC1 and PC2. Finally, the Tajik dataset overlaps partially with the Myanmar group and minimally also with the Afghan group.

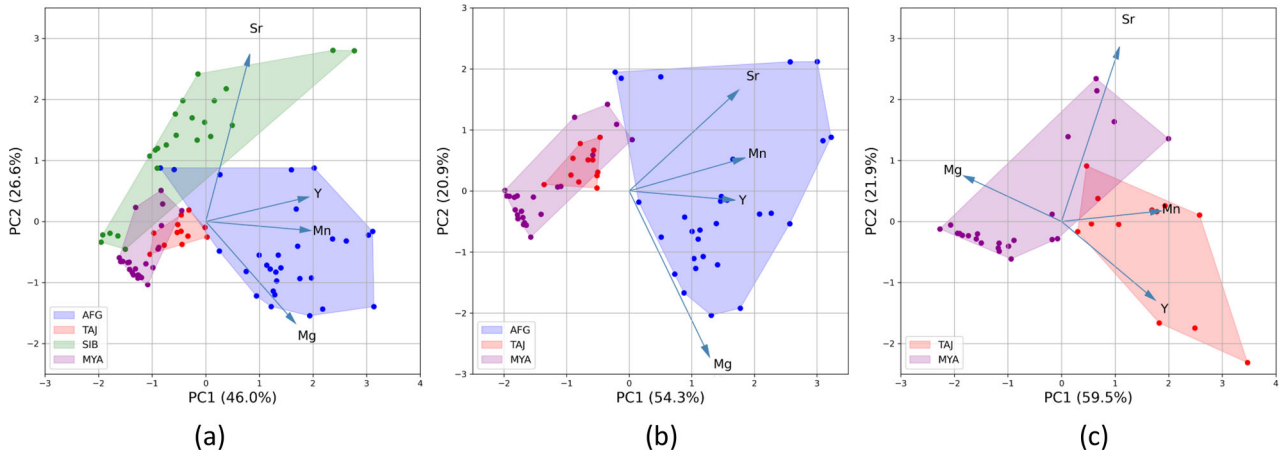

Fig. 5 **a** PC2 vs PC1 biplot obtained from PCA analysis on μ-PIXE data acquired on calcite crystals from all geological reference samples. **b** Same as (**a**) but with the data of Siberian provenance excluded. **c** Same as (**b**) but with the data of Afghan provenance excluded. The percentage of explained variance for each PC is reported in brackets

One of the main limitations in our current provenance protocol based on the study of diopside and pyrite is its poor discrimination power between Afghan, Tajik and Myanmar provenances. Applying PCA to the calcite dataset of only these provenances (Fig. 5b), therefore excluding the Siberian one, the Afghan group is instead clearly distinguishable from both the Myanmar group, although a minimum overlap remains, and the Tajikistan group. This separation occurs mainly along the PC1 direction to which now all 4 variables (Sr, Mn, Mg, Y) contribute with similar weight. The overall explained variance covered is 75,4%. In contrast, the data from Tajikistan and Myanmar rocks remain largely overlapping. A similar group separation was also achieved with PCA on the diopside data; however, the further attempt to enhance the separation between Tajikistan and Myanmar by applying PCA to only their datasets failed [26]. In the calcite case, PCA calculated only on the Tajik and Myanmar dataset (Fig. 5c) shows a partial differentiation, majorly along the PC1 direction to which Mg and Mn, negatively correlated this time, contribute the most. The overall explained variance covered is 81,4%. The study of calcites therefore proves to be a useful step forward for the study of lapis lazuli provenance, as it is the only way found to potentially distinguish Tajik provenance from Myanmar provenance. This differentiation is possible only when the Siberian and Afghan dataset are excluded (as could be suggested by complementary information obtained from IBIL measurements or by the study of other mineral phases); whereas, the two groups are rather indistinguishable when considering the whole reference dataset in the PCA. These PCA calculations will be adopted also in the next sections on data from archaeological samples with unknown origin to try to infer their provenance.

4.2 Analysis of reference rocks: μ-IBIL

Luminescence spectra of calcite crystals present in the reference rocks were acquired during different measurement runs at the AN2000 accelerator of the INFN-LNL laboratory. As explained in Sect. 3, since the IBIL setup is not fixed but installed each time, a direct quantitative comparison between the absolute intensity of the luminescence bands can only be made between data acquired during the same measurement run; while, band ratio analysis and qualitative considerations apply to the entire dataset. Figure 6 shows a representative set of IBIL spectra of calcite for each provenance. All spectra are characterised by a main band centred around 620 nm, which is due to the Mn^{2+} activator substituting Ca^{2+} in distorted octahedral sites of the calcite structure [28]. It is known from the literature on cold-cathodoluminescence [29, 30] and thermoluminescence [31] studies on calcite that under certain conditions the intensity of this band is linearly proportional to the Mn^{2+} content. This behaviour is expected at low concentrations of Fe^{2+} (< 1000 ppm) and Mn^{2+} itself, above which quenching and self-quenching mechanisms, respectively, start to occur (the concentration limits at which this phenomenon occurs are still debated) and the relationship is no longer linear [32]. Regarding the results of the IBIL measurements carried out in this study, a linear dependence with the total Mn content was observed, as shown in Fig. 7a), where the maximum intensity of the 620 nm band is plotted as a function of the Mn concentration obtained with μ-PIXE, the different colours referring to different provenances. The plotted data were acquired during the same measurement run. As discussed in the previous section, the Fe content measured with μ-PIXE was very low, always below 300 ppm in all the calcite crystals analysed, confirming the linear behaviour in such conditions. In the near UV part of the spectra, a second broad band with maximum at around 360 nm is visible in several samples for each provenance. According to the literature [33–35] this band could be attributed to the presence of Ce^{3+} substitutions at calcium sites. Cerium was not detected by μ-PIXE, but this could be due to its very low concentration. A few tens of ppm of Ce are sufficient to induce a luminescence signal [35], but not to be detected above the detection limit of the PIXE in the energy region of emission of Ce-L lines (LOD about 300 ppm at the LNL-INFN setup for this element). Another hypothesis reported by scholars [29, 36] is that this broad band is a result of intrinsic luminescence. For our

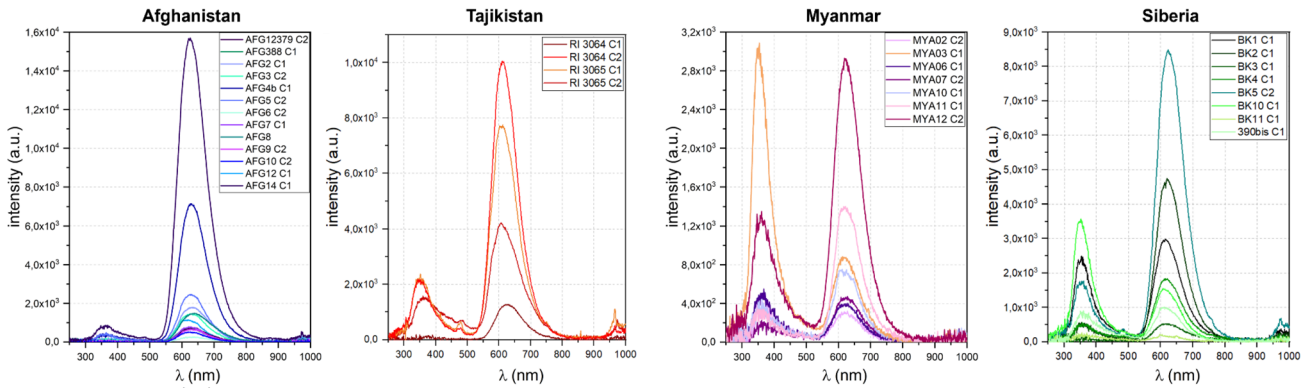

Fig. 6 Selection of representative μ-IBIL spectra of calcite crystals in different samples (from Afghanistan, Tajikistan, Myanmar, and Siberia). The integration time for each spectrum was set to 60 s

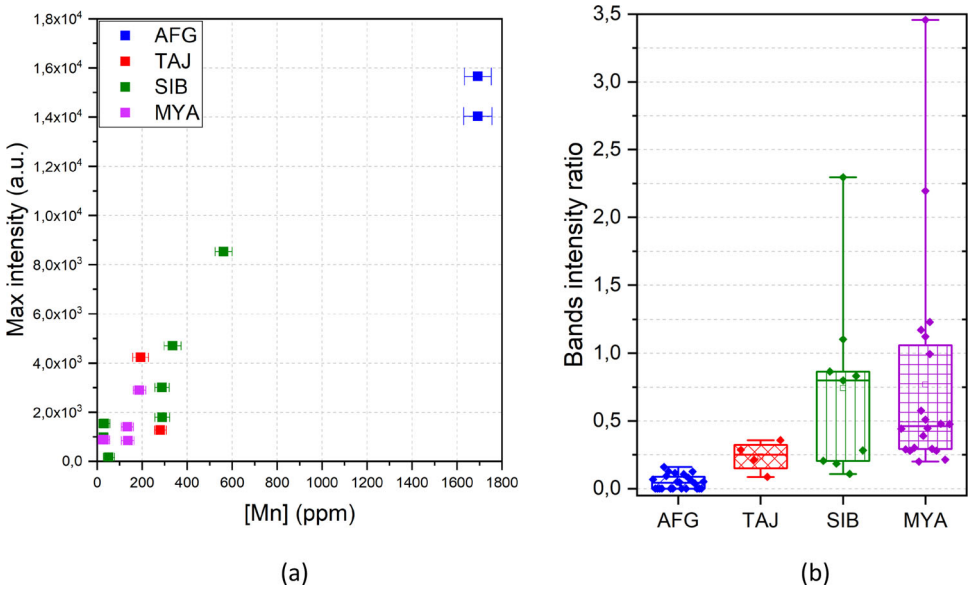

Fig. 7 **a** Maximum intensity of the 620 nm band (acquisition time 60 s) as a function of the Mn concentration obtained with μ-PIXE measurements on the same crystal. All the points were acquired in the same measurement run. **b** Intensity ratio between the 360 nm and the 620 nm bands, grouped by provenance

provenance study, it is interesting to note that there are some relevant differences in the ratio between the intensities of this minor band and the 620 nm band among the different provenances (Fig. 7b): Myanmar and Siberian calcites show the highest ratios, with some cases where the 360 nm band is even more intense than the Mn-activated band, while in Tajik and especially Afghan rocks this ratio is rather low (in 11 of the 24 Afghan calcites examined the 360 nm band is below the sensitivity of the instrument, and the ratio is therefore set to 0). This characteristic can be exploited as a provenance marker, particularly in the differentiation between the Afghan and Myanmar provenances, which are well distinguished in the boxplot of Fig. 7b. The ratio can also help in the usually difficult differentiation between Myanmar and Tajik lapis lazuli, even if the ranges of values show a partial overlap. Furthermore, μ-IBIL measurements are typically much faster than μ-PIXE measurements, thereby this provenance marker could be exploited to have a first rapid indication of provenance, especially in contexts where time for measurements is limited.

Other smaller peaks are sometimes visible in the spectra: one at about 480 nm and one at about 750 nm, which are often found together. According to the literature [35], we can assume that they correspond to the bands produced by the Dy^{3+} activator in calcite (the third peak at 580 nm typical of this activator could be covered by the slope of the main band at 620 nm). Finally, in some spectra, the 620 nm band does not exhibit a smooth top, but rather a sequence of small peaks with very poor resolution. This sequence could be hypothesised as the sequence of narrow bands produced by the Sm^{3+} activator in calcite. According to the literature, these bands can be found at 601 nm, 614 nm, 626 nm and 644 nm [36]. However, due to the low resolution, these individual peaks could not be resolved in our spectra. As in the case of Ce, the elements Dy and Sm were also not detected by μ-PIXE, probably due to their minimal amounts. Since these small secondary bands were observed in at least one sample for each provenance, they cannot be used as markers.

Table 2 Quantitative results for 6 calcite crystals in the 4 lapis lazuli fragments from Shahr-i Sokhta measured with μ-PIXE analysis and SEM–EDX (only for Mg). The SEM–EDX analysis provided the values as MgO in wt%, which were subsequently converted to Mg contents in ppm to facilitate comparison; the limit of detection (LOD) was not available. Concentration values and associated errors are reported, together with the relative limit of detection in case of μ-PIXE data

Sample	Area	Mg	Mn		Sr		Y	
		Conc ± err (ppm)	Conc ± err (ppm)	LOD (ppm)	Conc ± err (ppm)	LOD (ppm)	Conc ± err (ppm)	LOD (ppm)
SiS-4	C1	6400 ± 300	716 ± 6	3	1010 ± 40	21	120 ± 20	19
SiS-7	C1	17,800 ± 700	450 ± 4	4	540 ± 20	16	54 ± 8	16
SiS-7	C2	16,000 ± 1000	610 ± 6	4	700 ± 30	17	43 ± 13	13
SiS-178	C1	4800 ± 400	1195 ± 12	4	320 ± 40	39	140 ± 30	42
SiS-304	C1	14,500 ± 700	589 ± 8	5	770 ± 50	33	210 ± 30	24
SiS-304	C2	14,600 ± 500	568 ± 10	5	580 ± 60	40	150 ± 40	37

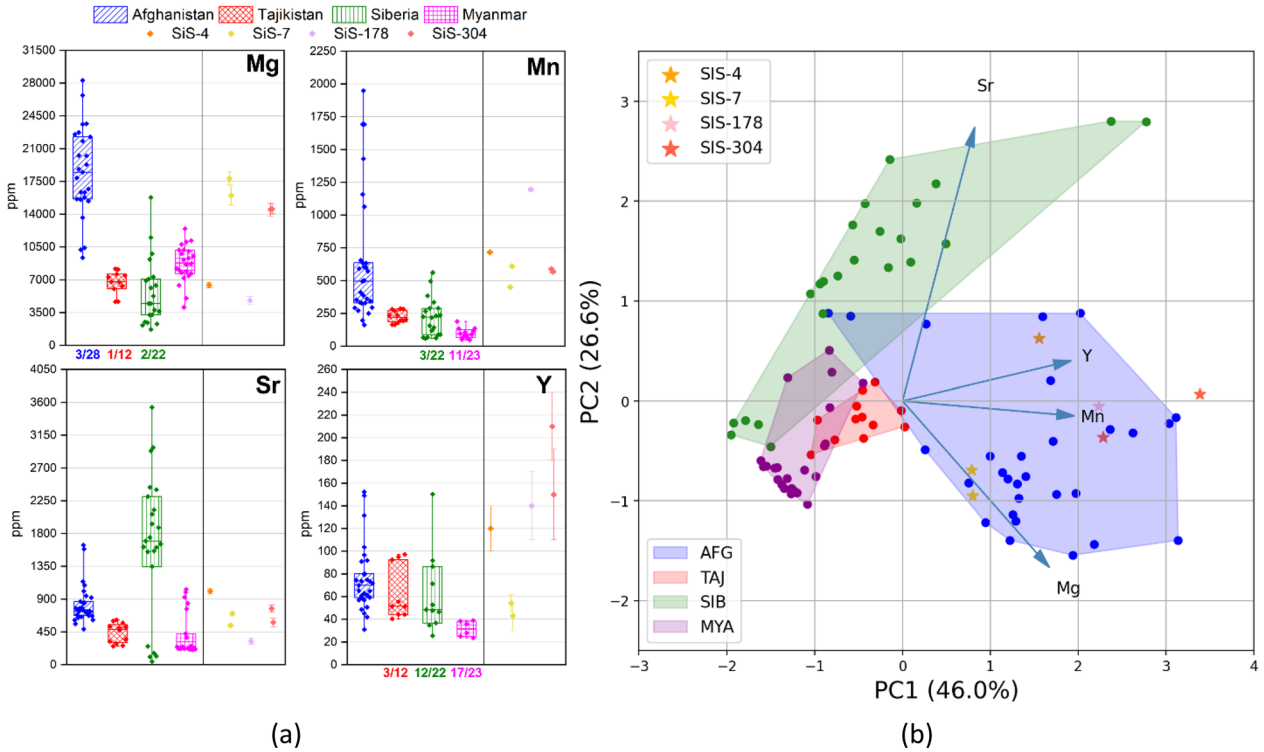

Fig. 8 **a** μ-PIXE results for trace elements concentration in calcite, comparing results from Shahr-i Sokhta lapis lazuli waste fragments (shown as single measured values with related error bar) to data from the other reference geological samples, grouped by provenance area. The box plots represent the dispersion of the experimental points: the median line and the two percentile values 0.25 and 0.75. The number of measurements below the limit of detection (LOD) with respect to the total number of crystals measured for each provenance is reported below the x-axis. **b** PC2 vs PC1 biplot obtained from PCA analysis on calcite μ-PIXE data from all geological reference samples. μ-PIXE data from Shahr-i Sokhta samples are projected on the PCs space

4.3 Case study 1: working fragments from Shahr-i Sokhta (Iran)

The results obtained in the previous sections were used to investigate the provenance of the raw material of four lapis lazuli fragments found at the site of Shahr-i Sokhta (Iran, 3rd millennium BCE). The measurements were conducted at the Surrey Ion Beam Centre, as described in Sect. 3, and only μ-PIXE data were considered for the analysis. Table 2 presents the concentration values of the most relevant elements for provenance discrimination: Mg, obtained via SEM–EDX, and Mn, Sr and Y, derived from μ-PIXE analysis. The concentration of these four elements is also presented in box plots in Fig. 8a in comparison with reference geological samples from our database, as discussed in Sect. 4.1. All the μ-PIXE calcite data of the Shahr-i Sokhta fragments are reported in the *Supplementary Material (*Online Resource 1*)*. Figure 8b shows the Principal Component 2 (PC2) vs PC1 biplot as in Fig. 5a on which score values calculated from the data of Shahr-i Sokhta samples are plotted after a scaling procedure using the same mean and standard deviation as the database model.

Table 3 Quantitative results for the 2 calcite crystals analysed in the Tanis tessera with μ-PIXE. Concentration values and associated errors are reported together with the relative limit of detection (LOD)

Sample	Area	Mg		Mn		Sr		Y	
		Conc ± err (ppm)	LOD (ppm)	Conc ± err (ppm)	LOD (ppm)	Conc ± err (ppm)	LOD (ppm)	Conc ± err (ppm)	LOD (ppm)
Tanis tessera	C1	11,000 ± 3000	1659	840 ± 70	58	1320 ± 50	21	130 ± 30	19
Tanis tessera	C2	10,000 ± 1000	908	970 ± 50	34	1300 ± 30	16	95 ± 13	16

Each sample presents a different combination of concentrations of the four provenance marker elements, suggesting the use of different rocks in the workshop from which these fragments were carved. In particular, samples SiS-7 and SiS-304 exhibit the highest concentration of Mg (minimum value 14,500 ± 700 ppm) and a similarly abundant concentration of Mn (in the range 440–630 ppm), which are incompatible with the Tajik dataset and, in the case of Mn, also with the Myanmar dataset, considering an interval of three standard deviations. The samples differ in their Y concentration, with sample SiS-304 exhibiting the highest Y content of all the samples (maximum of 210 ± 30 ppm); while, SiS-7 has the lowest content of this element (43 ± 13 ppm). In contrast, samples SiS-4 and SiS-178 exhibit a reduced Mg concentration (in the range of 4000–7000 ppm), and the highest concentrations of Mn, exceeding the threshold identified as an Afghan weaker marker (Mn > 670 ppm). The Y content is abundant in both samples, with concentrations above 100 ppm, but the relatively high values of the associated error do not allow to exclude provenances on the basis of this element. Finally, the Sr value was observed to be relatively low in all the four samples, with a maximum value of 1010 ± 40 ppm. Considering the single element concentration data, it can be suggested an Afghan provenance for the raw material of samples SiS-4 and SiS-178; while, an uncertainty remains between Afghanistan and Siberia for fragments SiS-7 and SiS-304. The application of PCA in this case facilitates the assessment of provenance by exploiting the correlation between the various elements. Figure 8b clearly demonstrates that for all samples, the best compatibility is with respect to the Afghan rocks dataset, thereby excluding the Siberian origin with good confidence for samples SiS-7 and SiS-304.

A comparison of these results with those presented in [13], which deals with the study of diopside and pyrite mineral phases in the same samples, reveals that the investigation of calcite in some cases reinforced the proposed provenance attribution by providing independent proofs, while in others it clearly resolved the ambiguity that was present on the attribution. For instance, the Afghan origin of the raw materials of fragments SiS-4 and SiS-304 was confirmed, as previously suggested by the identification of Afghan weaker markers in diopside crystals (5 out of 6 markers for SiS-4 and 3 out of 6 for SiS-304), and in pyrite crystals (phase present only in sample SiS-4). This proves the reliability of the provenance discriminating power of calcite analysis and the compatibility of the two approaches. Conversely, for fragments SiS-178, an uncertainty between Afghanistan and Myanmar provenance was left in the previous study, since only pyrite crystals were present, while in sample SiS-7, neither diopside nor pyrite crystals suitable for the study were available, thus leaving no possibility of attribution. The calcite results for these two fragments enabled us to infer an univocal indication of provenance of their raw materials, adding evidence to the work of [13] in confirming that the majority of the source material processed at Shahr-i Sokhta is likely to have an Afghan origin.

4.4 Case study 2: tessera from Tanis (Egypt)

Although the study of several mineralogical phases offers a more comprehensive perspective when comparing a certain artefact with the reference rocks dataset, the calcite analysis alone can be sufficient to ascertain the provenance. The study of the lapis lazuli tessera described in Sect. 2.2, retrieved in the Ancient Egyptian city of Tanis, proves this concept. The results of calcite are presented and compared to the standard methodology of the provenance protocol, applied here for the first time to the study of this tessera. We will initially consider the μ-PIXE results on the two calcite crystals in the tessera. The concentrations of the relevant elements are presented in Table 3 and in the form of boxplots in Fig. 9a. All the μ-PIXE calcite data of the tessera are reported in the *Supplementary Material (*Online Resource 1*)*. Figure 9b shows the score values calculated from these data plotted on the Principal Component 2 (PC2) vs PC1 biplot of Fig. 5a, after a scaling procedure using the same mean and standard deviation as the database model.

The tessera displays a considerable quantity of all the elements relevant for the provenance attribution. The minimum values for Mg (9800 ± 1400 ppm), Sr (1300 ± 30 ppm), and Y (95 ± 13 ppm) are however compatible with all four provenances, considering an interval of three standard deviations. In contrast, the concentration of Mn (minimum value 840 ± 70 ppm) exceeds the threshold identified as an Afghan weaker marker (Mn > 670 ppm), suggesting that Afghanistan represents the most probable source for the raw material of the tessera. The same conclusion can be reached by examining the PCA data plot, which combines the information carried by these variables. This plot shows that the PC1 and PC2 values calculated for the tessera are uniquely compatible with those of the Afghan dataset.

μ-IBIL spectra were also collected from the same calcite crystals (Fig. 10a) to evaluate the presence of other provenance markers. The intensity ratio between the two luminescence bands at 360 nm and 620 nm was calculated and it was compared with

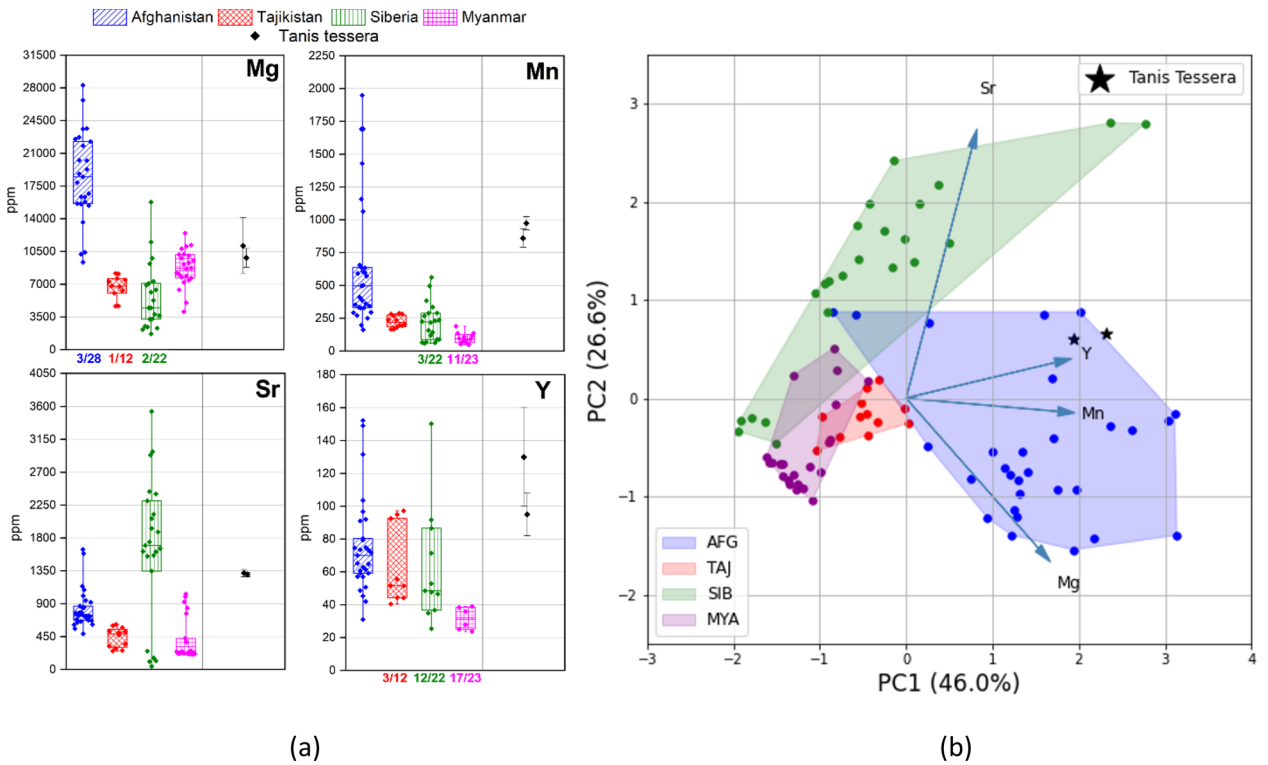

Fig. 9 **a** μ-PIXE results for trace elements concentration in calcite, comparing results from the lapis lazuli tessera from Tanis (shown as single measured values with related error bar) to data from the other reference geological samples, grouped by provenance area. The box plots represent the dispersion of the experimental points: the median line and the two percentile values 0.25 and 0.75. The number of measurements below the limit of detection (LOD) with respect to the total number of crystals measured for each provenance is reported below the x-axis. **b** PC2 vs PC1 biplot obtained from PCA analysis on calcite μ-PIXE data from all geological reference samples. μ-PIXE data from Tanis tessera are projected on the PCs space

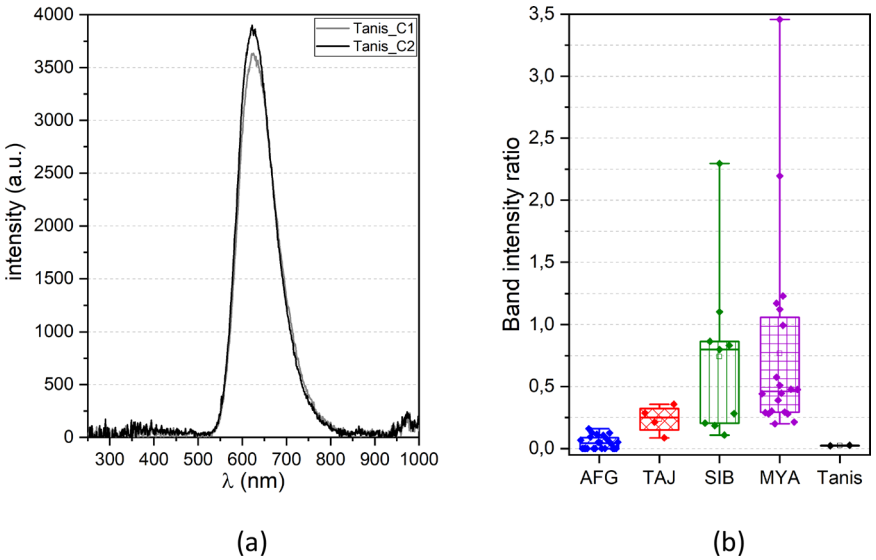

Fig. 10 **a** μ-IBIL spectra of calcite crystals in the Tanis tessera. The integration time for each spectrum was set to 60 s. **b** Intensity ratio between the 360 nm and the 620 nm bands, divided by provenance and compared with the values from the Tanis tessera

the corresponding values of the reference rocks dataset (discussed in Sect. 4.2), as shown in Fig. 10b**.** The ratio values are very close to zero and comparable only with those of the Afghan group, thereby confirming the attribution inferred by μ-PIXE results in an independent manner.

The provenance protocol described in [4] was applied for comparison. First, the alteration state of the pyrite crystals was evaluated exploiting SEM-BSE images acquired during the pre-characterisation phase: all the crystals observed in the tessera were well-preserved (some examples are reported in Fig. 11a) and without the presence of oxide-hydroxide minerals (which are typical alteration products of pyrite [37]), leading to the exclusion of the Siberian origin. In fact, Siberian rocks always contain strongly altered pyrite crystals, even in freshly cut rocks. In the following step of the protocol, the concentrations of Ni and Cu traces

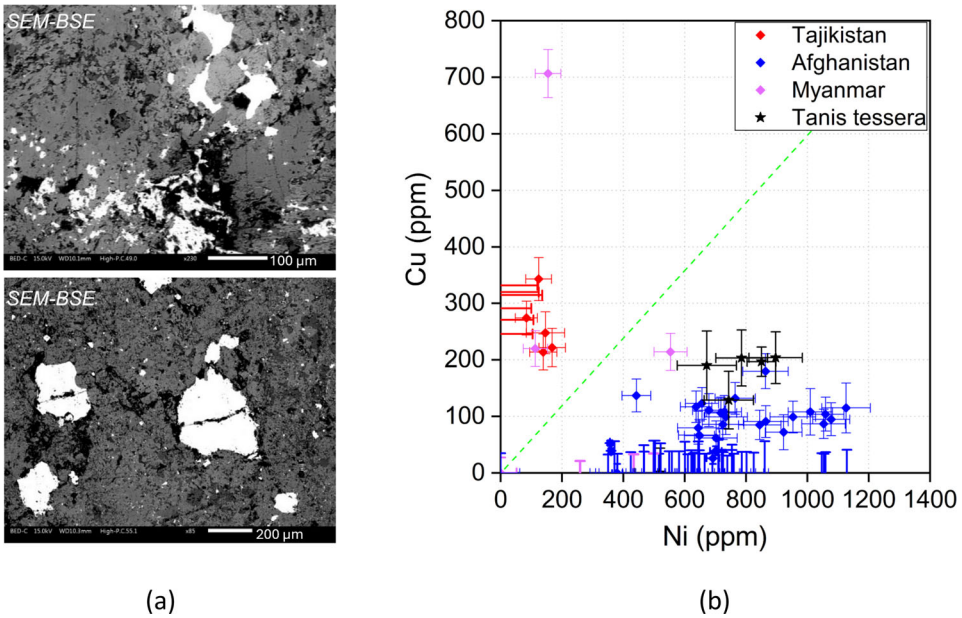

Fig. 11 **a** Examples of SEM-BSE images for Tanis tessera, the white homogeneous crystals are pyrite minerals well-preserved.**b** μ-PIXE results for copper and nickel trace elements in five crystals of pyrite in the lapis lazuli tessera from Tanis compared to data from the Tajikistan, Afghanistan and Myanmar reference geological samples [38]. All the μ-PIXE data of Tanis tessera are reported in the *Supplementary Material (*Online Resource 2*)*

in pyrite obtained with μ-PIXE analysis are compared with those of the Tajik and Afghan datasets (the Myanmar provenance is indistinguishable by these two elements), as shown in Fig. 11b. Since the traces in the pyrites of the Tanis tessera respect the condition $Cu < 0.6 \cdot Ni$, the Tajik provenance can be excluded, leaving an uncertainty between Afghanistan and Myanmar provenances.

In the final step of the protocol, trace elements within diopside are considered, in particular Ti, V, Cr, Mn and Zn, in order to evaluate the presence of Afghan or Myanmar weaker markers. The box plots related to the concentration of these elements are shown in Fig. 12a. The diopside crystals in the Tanis tessera present high amounts of Ti (minimum value 2720 ± 70 ppm) and Mn (minimum value 660 ± 30 ppm) well above the values identified as Afghan weaker markers (Ti > 800 ppm and Mn > 310 ppm). In addition, in 5 out of 6 crystals the Cr content is also above 75 ppm, another characteristic Afghan weaker marker. Zn and V are not discriminating elements in this case, having concentrations compatible with both Afghan and Myanmar datasets. μ-IBIL spectra collected on the same diopside crystals (a representative selection is shown in Fig. 12**b**) reveal a final clue for the Afghanistan attribution of the raw material of the tessera, that is the presence of the characteristic luminescence band at 770 nm, another feature observed only in Afghan rocks.

A side comment can be made regarding strontium. A high amount of Sr in diopside crystals is a distinctive feature of Siberian rocks and the threshold Sr > 234 ppm (updated in [40]) was identified as a weaker marker of this provenance in the protocol. In 2 of the 6 diopside crystals of Tanis tessera, the amount of Sr measured with μ-PIXE is slightly above this threshold (see Fig. 12a), resulting in an apparent conflict with the other provenance markers found. This could be explained by a probable incomplete characterisation of the variability of Sr content in diopside of Afghan rocks and reveal a relative applicability of this specific weaker marker. Moreover, similar situations with a high concentration of Sr in the diopside of archaeological samples showing other markers for attributing the material to Afghanistan have already been encountered in other case studies [3, 8].

The compatibility of the raw material of the Tanis tessera (1050–700 B.C., XXI-XXII dynasties) with the Afghan dataset revealed by this study reinforces the scientific evidence that trading occurred between Afghanistan and Egypt during the first millennium BCE, despite the approximately 4000 km distance between the two locations. The result is in accordance with the findings of the few scientific studies on the provenance of Egyptian artefacts made of lapis lazuli that are currently available in literature [1, 3].

5 Conclusions

The μ-PIXE and μ-IBIL analysis of calcite crystals in lapis lazuli revealed compositional and luminescence characteristics that can be exploited to introduce new possibilities for investigating the provenance of this rock. The analysis of a large set of reference rocks from four different origins (Afghanistan, Tajikistan, Siberia and Myanmar) evidenced that calcite from Afghan rocks has the highest magnesium and manganese content, in particular Mg > 18,000 ppm and Mn > 670 ppm were proposed as candidate weaker markers for this provenance. High levels of strontium, on the other hand, appear to be a distinctive feature of Siberian calcite, and Sr > 1740 ppm has been proposed as a Siberian potential weaker marker. Furthermore, Principal Component Analysis was employed to enhance the discrimination power derived from the correlation of the trace contents of Mg, Mn, Sr and Y. This analytical method proved to be extremely useful in achieving a good discrimination between the four provenances, and particularly in differentiating between the Tajikistan and Myanmar groups, when the Siberian and Afghan dataset are excluded from the calculation. This represents

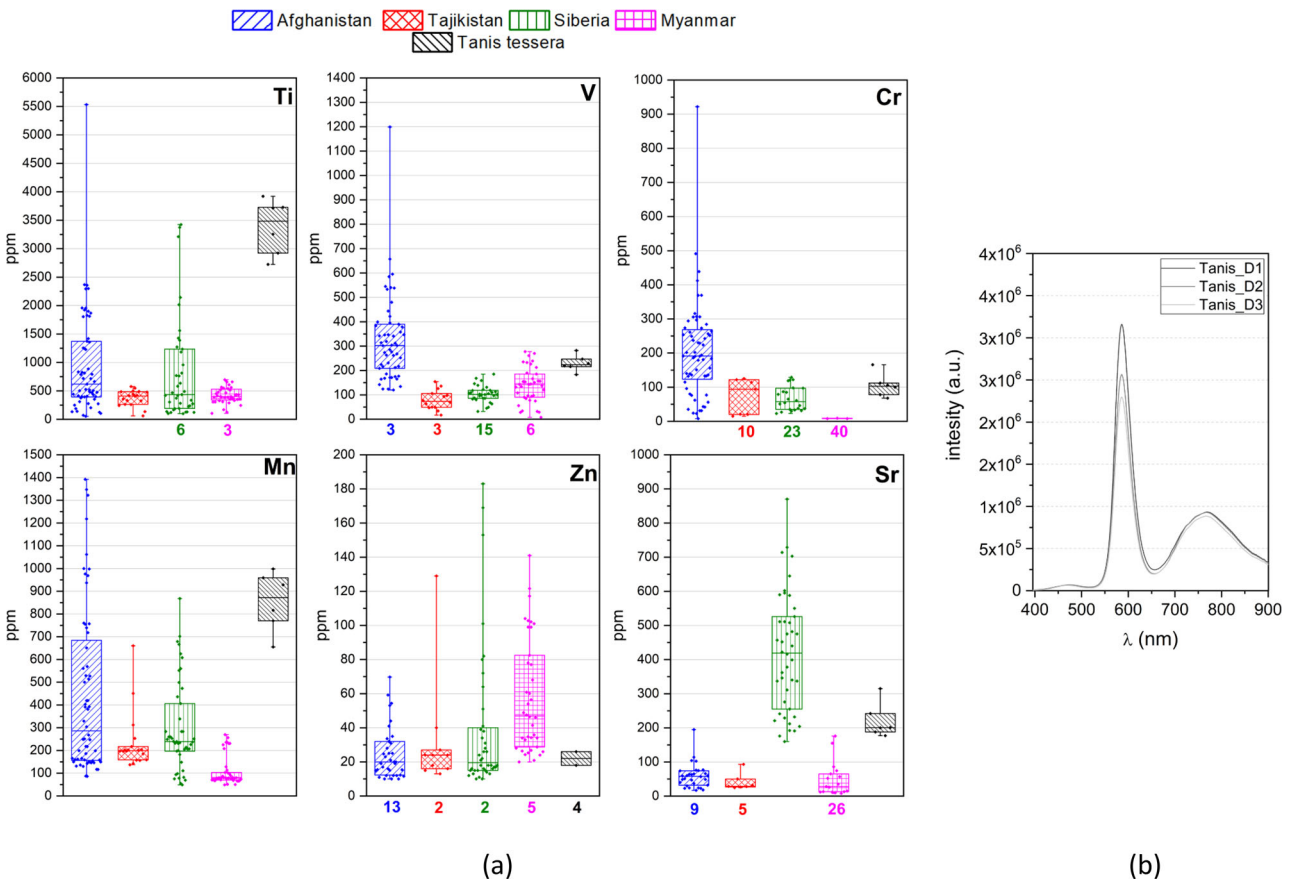

Fig. 12 **a** μ-PIXE results for trace elements concentration in diopside, comparing results from the lapis lazuli tessera from Tanis to data from the other reference geological samples [39], grouped by provenance area. The box plots represent the dispersion of the experimental points: the median line and the two percentile values 0.25 and 0.75. The values under the x-axis represent the number of measurements below the limit of detection (LOD). All the μ-PIXE data of Tanis tessera are reported in the *Supplementary Material (*Online Resource 3). **b** Representative μ-IBIL spectra of calcite crystals in the Tanis tessera. The integration time for each spectrum was set to 60 s

a significant advance over previous studies of the diopside and pyrite phases within lapis lazuli from the same set of rocks, which were unable to effectively differentiate these two groups, even when the other provenances are ruled out from the PCA. With regard to the study of calcite luminescence, the principal difference found in the calcite spectra was related to the ratio between the intensity of the minor broad band centred at about 360 nm and that of the major band centred at 620 nm. The highest ratios were observed in calcites from Myanmar and Siberia, with cases where the 360 nm band was even more intense than the main band (ratio > 1), while in Tajik and especially Afghan rocks this ratio was markedly lower (in 11 of the 24 Afghan calcites analysed with μ-IBIL the 360 nm band was not detected). This ratio can thus be exploited as a further provenance marker, particularly for the differentiation between Afghan and Myanmar origins which showed the largest difference, but also between Myanmar and Tajik lapis lazuli, even if the ranges of values show a partial overlap. This information could eventually overcome the PIXE difficulties in the discrimination between these last two groups. Furthermore, the reduced acquisition time required for μ-IBIL measurements makes this marker a more rapid method, in comparison with μ-PIXE, for obtaining an initial indication of provenance.

In the second part of this study, the calcite provenance markers were employed to investigate the origin of four lapis lazuli fragments discovered at Shahr-i Sokhta (Iran, 3rd millennium BCE) and a lapis lazuli tessera from the city of Tanis (Egypt, 1050–700 BCE, XXI-XXII dynasties). The study of calcite proved to be a reliable and effective method for determining the origin of the samples raw material. In addition to supporting the attribution hypothesis obtained by the application of the standard provenance protocol, it also resolved attribution issues that remained unanswered in previous studies. For all the samples, the results of the analysis showed the highest degree of compatibility with the Afghan dataset, among the four provenances considered in the reference rocks database. This finding suggests that the quarries of Afghanistan are the most probable source of the raw material used to carve the samples discovered in these two ancient sites, and it provides scientific evidence to support the archaeological investigation about the trade routes connecting these sites with their suppliers area.

Supplementary Information The online version contains supplementary material available at https://doi.org/10.1140/epjp/s13360-025-06095-5.

Acknowledgements The authors wish to warmly thank IPERION CH (Grant Agreement n. 654028) and IPERION HS (Grant Agreement n. 871034) EU Transnational Access programmes for the financial support of SIBILLA project; and acknowledge the support by the RADIATE project funded by the European Union's Horizon 2020 research and innovation program under grant agreement No. 824 096. The EQUIPEX New AGLAE research program (n. ANR-10-EQPX-22, French Ministry of Research) is acknowledged. The GFI: Grant For Internationalisation promoted by the Physics Department of the University of Torino is also acknowledged for the financial support. The authors wish to thank Prof. Luca Martire for the availability of the Cold-CL apparatus, and the scientific laboratories of the Centro Conservazione e Restauro "La Venaria Reale", Torino (Italy) for the SEM instrumentations. The authors are also deeply grateful to Prof. E. Bresciani for her availability.

Funding Open access funding provided by Università degli Studi di Torino within the CRUI-CARE Agreement.

Data Availability Statement All relevant data generated or analysed during this study are included in this manuscript or available at Zenodo public repositories as indicated; additional information can be granted upon reasonable request to the authors. The manuscript has data included as electronic supplementary materials.

Declarations

Conflict of interest The authors have no affiliations with or involvement in any organisation or entity with any financial interest or non-financial interest in the subject matter or materials discussed in this manuscript.

References

1. T. Calligaro, Y. Coquinot, L. Pichon, G. Pierrat-Bonnefois, P. De Campos, A. Re, D. Angelici, Nucl. Instrum. Methods Phys. Res. Sect. B **318**, 139–144 (2014). https://doi.org/10.1016/j.nimb.2013.06.063
2. A. Re, D. Angelici, A.L. Giudice, J. Corsi, S. Allegretti, A.F. Biondi, G. Gariani, S. Calusi, N. Gelli, L. Giuntini, M. Massi, F. Taccetti, L. La Torre, V. Rigato, G. Pratesi, Nucl. Instrum. Methods Phys. Res. Sect. B **348**, 278–284 (2015). https://doi.org/10.1016/j.nimb.2014.11.060
3. A.L. Giudice, D. Angelici, A. Re, G. Gariani, A. Borghi, S. Calusi, L. Giuntini, M. Massi, L. Castelli, F. Taccetti, T. Calligaro, C. Pacheco, Q. Lemasson, L. Pichon, B. Moignard, G. Pratesi, M.C. Guidotti, Archaeol Anthropol Sci **9**(4), 637–651 (2017). https://doi.org/10.1007/s12520-016-0430-0
4. L. Guidorzi, A. Re, M. Magalini, D. Angelici, A. Borghi, G. Vaggelli, F. Fantino, V. Rigato, L. La Torre, Q. Lemasson, C. Pacheco, L. Pichon, B. Moignard, A.L. Giudice, Eur Phys J Plus (2023). https://doi.org/10.1140/epjp/s13360-023-03768-x
5. G. Hermann, Iraq **30**(1), 21–57 (1968). https://doi.org/10.2307/4199836
6. M. Casanova, Le lapis-lazuli dans l'Orient Ancien: production et circulation du Néolithique au IIe millénaire av. J.-C. (Editions du Comité des travaux historiques et scientifiques, Paris, 2013).
7. M. Vidale, A. Lazzari, Lapis lazuli bead making at Shahr-i Sokhta: Interpreting craft production in a urban community of the 3rd millennium BC (Treviso, Edizioni Antilia, 2017).
8. M. Magalini, L. Guidorzi, A. Re, D. Frenez, K.D. Williams, K.A. Douglas, N.S. al-Jahwari, Q. Lemasson, C. Pacheco, L. Pichon, B. Moignard, A. Lo Giudice. J. Archaeol. Sci. **174** , 106131 (2025). https://doi.org/10.1016/j.jas.2024.106131
9. L. Guidorzi, Physico-chemical characterization of diopside in lapis lazuli: a study from luminescence activators and quenchers to material provenance investigations, (PhD thesis, Chemical and Materials Sciences, Università degli studi di Torino, 2021) pp. 17–18.
10. A. Lo Giudice, A. Re, S. Calusi, M. Massi, P. Olivero, G. Pratesi, M. Albonico, E. Conz, Anal. Bioanal. Chem. **395**, 2211–2217 (2009). https://doi.org/10.1007/s00216-009-3039-7
11. G. Vaggelli, L.E. Sebar, A. Borghi, R. Cossio, A. Re, F. Fantino, A.L. Giudice, Improvements to the analytical protocol of lapis lazuli provenance: first study on Myanmar rock samples. Eur. Phys. J. Plus (2019). https://doi.org/10.1140/epjp/i2019-12523-4
12. M. Tosi, M. Piperno, Expedition Magazine **16**, 15–23 (1973)
13. L. Guidorzi, M. Magalini, A. Re, A. Borghi, M. Vidale, L. La Torre, V. Rigato, Q. Lemasson, C. Pacheco, L. Pichon, B. Moignard, P. Couture, V. Palitsin, A. Lo Giudice. Provenance attribution of lapis lazuli rocks processed at the Bronze Age archaeological site of Shahr-i Sokhta. Journal of Archaeological Science 2024, under review.
14. W.A. Deer, R.A. Howie, J. Zussman, An introduction to the rock-forming minerals (3rd ed.) (The Mineralogical Society of Great Britain and Ireland, London, 2013), pp. 451–453. https://doi.org/10.1180/DHZ
15. J.F. Ziegler, M.D. Ziegler, J.P. Biersack, Nucl. Instruments Methods Phys. Res. B **268**(11–12), 1818–1823 (2010). https://doi.org/10.1016/j.nimb.2010.02.091
16. P. Boccaccio, D. Bollini, D. Ceccato, G.P. Egeni, P. Rossi, V. Rudello, M. Viviani, Nucl. Instrum. Methods Phys. Res. Sect. B **109**(110), 94–98 (1996). https://doi.org/10.1016/0168-583X(95)00891-8
17. G.W. Grime, M. Dawson, Nucl. Instrum. Methods Phys. Res. Sect. B **104**(1–4), 107–113 (1995). https://doi.org/10.1016/0168-583X(95)00401-7
18. A. Simon, C. Jeynes, R.P. Webb, R. Finnis, Z. Tabatabaian, P.J. Sellin, M.B.H. Breese, D.F. Fellows, R. van den Broek, R.M. Gwilliam, Nucl. Instrum. Methods Phys. Res. Sect. B **219–220**, 405–409 (2004). https://doi.org/10.1016/j.nimb.2004.01.091
19. G.W. Grime, O.B. Zeldin, M.E. Snell, E.D. Lowe, J.F. Hunt, G.T. Montelione, L. Tong, E.H. Snell, E.F. Garman, J. Am. Chem. Soc. **142**, 185–197 (2020). https://doi.org/10.1021/jacs.9b09186
20. N. Claessens, P. Couture, J. England, R. Vos, T. Hantschel, W. Vandervorst, A. Vantomme, J. Meersschaut, Surf. Interfaces **32**, 102101 (2022). https://doi.org/10.1016/j.surfin.2022.102101
21. L. Pichon, B. Moignard, Q. Lemasson, C. Pacheco, P. Walter, Nucl. Instrum. Methods Phys. Res. Sect. B **318**, 27–31 (2014). https://doi.org/10.1016/j.nimb.2013.06.065
22. L. Pichon, T. Calligaro, V. Gonzalez, Q. Lemasson, B. Moignard, C. Pacheco, Nucl. Instrum. Methods Phys. Res. Sect. B **348**, 68–72 (2015). https://doi.org/10.1016/j.nimb.2015.01.010

23. L. Pichon, T. Calligaro, Q. Lemasson, B. Moignard, C. Pacheco, Nucl. Instrum. Methods Phys. Res. Sect. B **363**, 48–54 (2015). https://doi.org/10.1016/j.nimb.2015.08.086
24. J.L. Campbell, N.I. Boyd, N. Grassi, P. Bonnick, J.A. Maxwell, Nucl. Instrum. Methods Phys. Res. Sect. B **268**(20), 3356 (2010). https://doi.org/10.1016/j.nimb.2010.07.012
25. A. Lo Giudice, A. Re, L. Guidorzi, M. Magalini (2024). Database of elemental concentration of calcite in lapis lazuli rocks of different provenances obtained by micro-PIXE (ver1.0) . Zenodo. https://doi.org/10.5281/zenodo.14055468
26. L. Guidorzi, A. Re, M. Magalini, A.L. Giudice, Nucl. Instrum. Methods Phys. Res. Sect. B **540**, 45–50 (2023). https://doi.org/10.1016/j.nimb.2023.04.007
27. Spyder program documentation https://docs.spyder-ide.org/current/index.html (accessed on November 28th, 2024).
28. W.L. Medlin, J. Chem. Phys. **30**, 451–458 (1959). https://doi.org/10.1063/1.1729973
29. D. Habermann, R.D. Neuser, D.K. Richter, Sed. Geol. **116**(1–2), 13–24 (1998). https://doi.org/10.1016/S0037-0738(97)00118-8
30. S. Cazenave, R. Chapoulie, G. Villeneuve, Mineral. Petrol. **78**, 243–253 (2003). https://doi.org/10.1007/s00710-002-0227-y
31. T. Calderon, P.D. Townsend, P. Beneitez, J. Garcia-Guinea, A. Millan, H.M. Rendell, A. Tookey, M. Urbina, R.A. Wood, Radiat. Meas. **26**, 719–731 (1996). https://doi.org/10.1016/S1350-4487(97)82886-7
32. M. Corazza, G. Pratesi, C. Cipriani, A. De Giudice, P. Rossi, E. Vittone, C. Manfredotti, E. Pecchioni, C. Manganelli del Fà, F. Fratini, Archaeometry **43**, 439–446 (2001). https://doi.org/10.1111/1475-4754.00026
33. R. Chapoulie, F. Bechtel, D. Borschneck, M. Schvoerer, G. Rémond, Scanning Microsc. **1995**(9), 18 (1995)
34. C.M. Macrae, N.C. Wilson, Luminescence database I—minerals and materials. Microsc. Microanal. **14**(2), 184–204 (2008). https://doi.org/10.1017/S143192760808029X
35. M. Gaft, R. Reisfeld, G. Panczer, Modern luminescence spectroscopy of minerals and materials, (Springer Mineralogy, 2015), pp. 60–66. https://doi.org/10.1007/978-3-319-24765-6
36. M. Pagel, V. Barbin, P. Blanc, D. Ohnenstetter, *Cathodoluminescence in geosciences: an introduction* (Springer, Berlin Heidelberg, 2000), pp.1–21
37. A. Re, D. Angelici, A. Lo Giudice, E. Maupas, L. Giuntini, S. Calusi, N. Gelli, M. Massi, A. Borghi, L.M. Gallo, G. Pratesi, P.A. Mandò, New markers to identify the provenance of lapis lazuli: trace elements in pyrite by means of micro-PIXE. Appl. Phys. A **111**(1), 69–74 (2013). https://doi.org/10.1007/s00339-013-7597-3
38. A. Lo Giudice, A. Re, L. Guidorzi, M. Magalini (2024). Database of elemental concentration of pyrite in lapis lazuli rocks of different provenances obtained by micro-PIXE (ver1.0) . Zenodo. https://doi.org/10.5281/zenodo.13902916
39. A. Lo Giudice, A. Re, L. Guidorzi, M. Magalini (2024). Database of elemental concentration of diopside in lapis lazuli rocks of different provenances obtained by micro-PIXE (ver1.0) . Zenodo. https://doi.org/10.5281/zenodo.13913431
40. M. Magalini, L. Guidorzi, A. Re, F. Tansella, F. Picollo, S. Sturari, P. Aprà, G. Herrmann, R. Law, Q. Lemasson, L. Pichon, B. Moignard, C. Pacheco, A. Lo Giudice, Micro-computed tomography and laser micro-ablation on altered pyrite in lapis lazuli to enhance provenance investigation: a new methodology and its application to archaeological cases. Eur. Phys. J. Plus **140**, 59 (2025). https://doi.org/10.1140/epjp/s13360-025-05988-9